Design of GaN/AlGaN/GaN Super-Heterojunction Schottky Diode

Sang-Woo Han, Jianan Song, and Rongming Chu

***Abstract*— We present a systematic study on the design of a novel GaN/AlGaN/GaN super-heterojunction Schottky diode. Through physics-based TCAD simulation, we discuss three important design aspects: 1) how to design a GaN/AlGaN/GaN structure to form a high-density 2-D electron gas and to scale it to multiple vertically stacked channels with less risk in reaching the critical thickness limited by the strain in epitaxy; 2) how to reach charge balance and how sensitive is the breakdown voltage with respect to the doping imbalance; and 3) how to ensure that the processes of depleting and accumulating electrons and holes in the structure are fast enough for practical power switching applications.**

***Index Terms*— Gallium nitride, GaN/AlGaN/GaN, multichannel, Schottky barrier diode, superjunction, TCAD.**

I. Introduction

OVER the past 10 years, advancements in GaN materials and devices have made GaN-based power devices a serious contender for power switching applications [1]. Meanwhile, the performance of Si-based power devices, especially the advanced superjunction MOSFETs, has also progressed significantly [2]. Combining the benefits of the wide bandgap GaN material and the advantages of the superjunction device design would lead to ultimate power switches with minimal power loss. Reported simulation performances show the great potential of GaN vertical superjunction for future power switching applications [3], [4]. A major challenge toward realizing the GaN vertical superjunction is to implement the p- and n-type pillars. For Si superjunction devices, this was done either by multiple epitaxial regrowth and implantation steps [5], or by a deep etch followed by sidewall epitaxial regrowth [6]. Regrowth of GaN epitaxy often resulted in unwanted impurities and defects at the regrowth interface [7], [8], causing difficulties in charge balance. Furthermore, when the defective regrowth interface is located in the high E-field region, a premature breakdown could occur. Ishida *et al.* reported the concept of natural superjunction based on polarization-induced 2-D electron gas (2DEG) and 2-D hole gas (2DHG) pairs in a single- and multichannel GaN/AlGaN/GaN heterostructures [9]. The lateral superjunction structure did not require any epitaxial regrowth. Questions that still need to be answered in this area include: 1) how to scale from 1 to 3 channels to a larger number of channels with high-density 2DEG in each channel and 2) how to ensure that the process of depleting and accumulating 2DEG/2DHG is fast enough for practical switching applications.

In this article, we discuss several key aspects in designing a GaN superjunction, through TCAD simulation of a GaN multichannel super-heterojunction (SHJ) Schottky diode, as shown in Fig. 1. The proposed new diode structure features: 1) vertical stacking of multiple 2DEG channels to minimize ON-resistance; 2) balanced p- and n-type doping to achieve the maximum voltage blocking capability; and 3) p-type ohmic contact to ensure proper switching behaviors. We used Silvaco ATLAS for this study. Model parameters used in this study are listed in Table I.

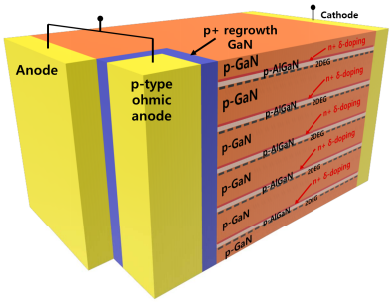

Fig. 1. Conceptual schematic of the proposed GaN/AlGaN/GaN multichannel SHJ Schottky diode.

TABLE I
Models and Parameters Used for TCAD Simulation

Physics	Model / parameter
Carrier statistics	Fermi-Dirac, incomplete ionization
Carrier transport	Drift-diffusion, concentration & field-dependent mobility [21]
Generation-recombination	Schokley-Read-Hall, Auger, and radiative
Breakdown	Selberherr impact ionization [22]
SRH lifetime	0.1 ns for electron [23] 6.5 ns for hole [24]
Activation energy	15 meV for donor 170 meV for acceptor
Radiative recombination rate	1.1×10^{-8} cm^3/s [25]

II. Design of GaN/AlGaN/GaN Epitaxial Structure for Stacking Multiple 2DEG Channels

In a conventional single-channel AlGaN/GaN structure, polarization field tilts the energy band, resulting in the transfer of electrons from surface donors to the AlGaN/GaN heterojunction, forming a high-density 2DEG channel without the need for intentional impurity doping [10]. In order to build SHJ with multiple 2DEG channels as shown in Fig. 2(a), stacking of multiple GaN/AlGaN/GaN structures are needed. Since surface donors cannot contribute sufficient and equal amount of electrons to each 2DEG channel in a GaN/AlGaN/GaN

Manuscript received October 12, 2019; revised November 11, 2019; accepted November 13, 2019. Date of publication December 13, 2019; date of current version December 30, 2019. The review of this article was arranged by Editor K. Alam. *(Corresponding author: Sang-Woo Han.)*

The authors are with the School of Electrical Engineering and Computer Science, The Pennsylvania State University, University Park, PA 16802 USA (e-mail: sxh1218@psu.edu).

Color versions of one or more of the figures in this article are available online at http://ieeexplore.ieee.org.

Digital Object Identifier 10.1109/TED.2019.2953843

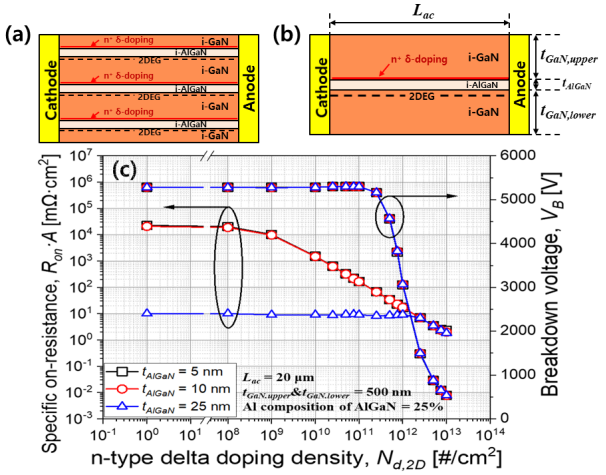

Fig. 2. (a) Cross-sectional schematics of GaN/AlGaN/GaN multichannel Schottky diode. (b) Single-channel Schottky diode used for simulation. (c) Dependence of $R_{ON} \cdot A$ and V_B on n-type delta-doping density for GaN/AlGaN/GaN single-channel Schottky diodes with different t_{AlGaN}.

structure where the 2DEG channel is far away from the surface, n-type delta-doping is often incorporated into the upper GaN/AlGaN interface to provide electrons needed by the 2DEG channel [11].

We performed a TCAD simulation of single-channel GaN/AlGaN/GaN Schottky diode structures shown in Fig. 2(b). The anode-to-cathode spacing (L_{ac}) was kept at 20 μm. An AlGaN layer was sandwiched between two GaN layers, each having a thickness of 500 nm. The AlGaN layer had an Al composition of 25%. The AlGaN layer thickness (t_{AlGaN}) was varied from 5 to 25 nm. The n-type delta-doping density ($N_{d,2\text{-D}}$) was varied from 0 to 1×10^{13} cm^{-2}. Specific ON-resistance ($R_{ON} \cdot A$) and breakdown voltage (V_B) were extracted from simulated forward and reverse I–V characteristics. Fig. 2(c) shows $R_{ON} \cdot A$ and V_B of the Schottky diode as a function of $N_{d,2\text{-D}}$ and different t_{AlGaN}.

Structures with t_{AlGaN} of 5 and 10 nm behaved similarly. Their $R_{ON} \cdot A$ were as high as 2×10^4 m$\Omega \cdot$cm^2 without sufficient amount of n-type delta-doping. This is because the polarization dipole across the AlGaN layer is not strong enough to transfer electrons from the surface states or the valance band of the upper GaN layer to form the 2DEG channel. Adding n-type delta-doping at the upper GaN/AlGaN interface effectively contributed electrons to the 2DEG channel, thereby lowering the $R_{ON} \cdot A$ down to 2.3 m$\Omega \cdot$cm^2 at delta-doping density of 1×10^{13} cm^{-2}. However, increasing delta-doping density also dramatically reduced the V_B from 5.3 kV to about 533 V. This was because under reverse bias, the added high density of donors became high density of positive fixed charges in the depletion region, resulting in high E-field. When the AlGaN thickness was increased to 25 nm, polarization dipole across the AlGaN became strong enough to transfer electrons from the valence band of the upper GaN layer to the conduction band of the lower GaN layer, forming 2DHG at the upper GaN/AlGaN interface and 2DEG at the lower AlGaN/GaN interface. Consequently, low $R_{ON} \cdot A$ of 10 m$\Omega \cdot$cm^2 can be achieved without the need for n-type doping. Adding n-type delta-doping to this structure further reduced the $R_{ON} \cdot A$, but at the cost of decreasing V_B. Note that low $R_{ON} \cdot A$ and high V_B could be simultaneously achieved in this structure, when there was no n-type doping. This is because the 2DHG naturally balances the 2DEG, forming the so-called natural superjunction [9]. Practical implementation of the natural superjunction is limited by a few factors: 1) near valance trap states located at the upper GaN/AlGaN interface can affect the charge balance and the transient response [12]; 2) stacking multiple layers of thick AlGaN layer with large Al composition, which is needed to generate the 2DHG-2DEG pair, exceeds the critical thickness and causes film cracking [13], [14]; and 3) without p-type impurity doping, it is hard to form a p-type contacts to the 2DHG channel, which is needed to supply holes during switching as will be discussed in Section IV. In order to construct GaN/AlGaN/GaN SHJ with multiple 2DEG channels, we prefer a thin AlGaN layer with modest Al composition to avoid degradation of epitaxial material quality. With a thin AlGaN layer and modest Al composition, n-type doping is needed to form high-density 2DEG channels and achieve low $R_{ON} \cdot A$. However, n-type doping disturbs the charge balance and requires additional measures to recover the V_B.

III. Charge Balance for SHJ With Improved Breakdown Voltage

The degraded V_B can be recovered by adding p-type doping to balance the amount of positive and negative ionized impurities. In our proposed SHJ structure, we chose to use relatively thick upper ($t_{GaN.upper}$) and lower GaN layers ($t_{GaN.lower}$), so that only medium-low p-doping concentration is needed to balance the n-type delta-doping. The use of the medium-low p-type doping is favorable for reducing impurity scattering and maintaining high 2DEG mobility. In this section, we discuss simulated forward, reverse, and transient characteristics of charge-balanced SHJ Schottky diodes. A 5-nm-thick AlGaN barrier layer with 25% Al composition was used in this study. Mg was used as the p-type dopant, with the activation energy of 170 meV.

A. Effects of p-Type Doping on $R_{ON} \cdot A$ and V_B

Fig. 3(a) shows the simulated $R_{ON} \cdot A$ as a function of 3-D p-type doping concentration ($N_{a,3\text{-D}}$) with a different n-type delta-doping density ($N_{d,2\text{-D}}$). Considering the difficulty in p-type modulation doping due to the Mg memory effect, we assumed uniform p-type doping for the upper GaN layer, the AlGaN layer, and the lower GaN layer. The $N_{a,3\text{-D}}$ was varied from 0 to 1.2×10^{17} cm^{-3}. Different $N_{d,2\text{-D}}$ values of 2.5×10^{12} cm^{-2}, 5×10^{12} cm^{-2}, 7.5×10^{12} cm^{-2}, and 1×10^{13} cm^{-2} were chosen for the simulation. For a given $N_{d,2\text{-D}}$, $R_{ON} \cdot A$ increased with increasing $N_{a,3\text{-D}}$, mainly due to depletion of electrons by the p-type doping. At charge balance condition, i.e., when $N_{a,2\text{-D}}$ (the integration of $N_{a,3\text{-D}}$ over the entire GaN/AlGaN/GaN thickness) equals $N_{d,2\text{-D}}$, the $R_{ON} \cdot A$ were 35.2 m$\Omega \cdot$cm^2 ($N_{d,2\text{-D}} = 2.5 \times 10^{12}$ cm^{-2} and $N_{a,3\text{-D}} = 2.5 \times 10^{16}$ cm^{-3}), 10.9 m$\Omega \cdot$cm^2 ($N_{d,2\text{-D}} = 5 \times 10^{12}$cm^{-2} and $N_{a,3\text{-D}} = 5 \times 10^{16}$ cm^{-3}), 6.6 m$\Omega \cdot$cm^2 ($N_{d,2\text{-D}} = 7.5 \times 10^{12}$ cm^{-2} and $N_{a,3\text{-D}} = 7.5 \times 10^{16}$ cm^{-3}), and 5.7 m$\Omega \cdot$cm^2 ($N_{d,2\text{-D}} = 1 \times 10^{13}$ cm^{-2} and $N_{a,3\text{-D}} = 1 \times 10^{17}$ cm^{-3}), respectively. For a charge-balanced structure, as the doping level increases, the number of mobile carriers increases, resulting in lower $R_{ON} \cdot A$.

Fig. 3(b) shows the simulated V_B as a function $N_{a,3\text{-D}}$. Consistent with the superjunction theory, V_B reaches its maximum value at the charge balance condition. The maximum V_B value was 5.3 kV in this case, with anode-to-cathode spacing of 20 μm. Deviating from the charge balance point resulted

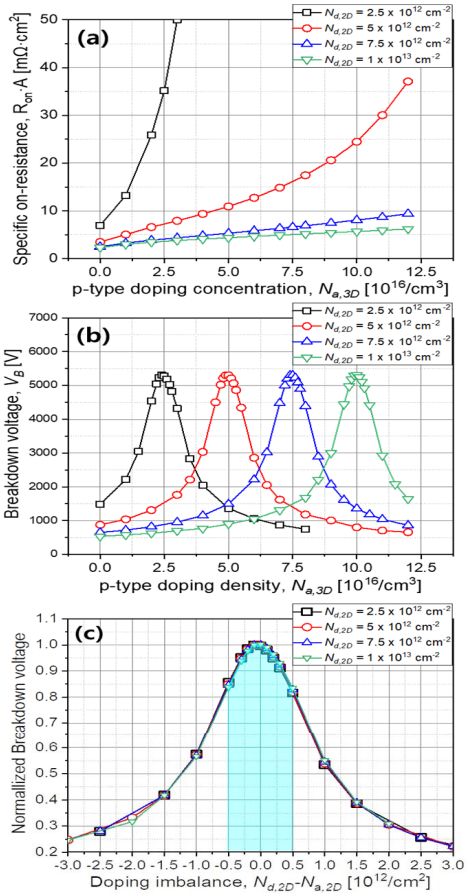

Fig. 3. Dependence of (a) $R_{ON} \cdot A$ and (b) V_B of charge-balanced GaN/AlGaN/GaN single-channel Schottky diodes on the p-type doping concentration [$N_{a,3\text{-D}}$]. (c) Sensitivity of the normalized V_B to doping imbalance [$N_{d,2\text{-D}} - N_{a,2\text{-D}}$].

in a rapid reduction of V_B. Fig. 3(c) shows the normalized breakdown voltage as a function of doping imbalance. About 80% of the maximum V_B can be maintained with up to 5×10^{11} cm^{-2} (in 2-D density), or 5×10^{15}cm^{-3} (in 3-D density), of doping imbalance.

B. Scaling of $R_{ON} \cdot A$ and V_B With Anode-to-Cathode Spacing

Fig. 4(a) shows the simulated reverse I–V characteristics of SHJ diodes with the L_{ac} varied from 1 to 100 μm. The simulated SHJ diodes had perfect charge balance, with $N_{d,2\text{-D}} = 1 \times 10^{13}$ cm^{-2} and $N_{a,3\text{-D}} = 1 \times 10^{17}$ cm^{-3}. Fig. 4(b) summarizes the dependence of $R_{ON} \cdot A$ and V_B on the L_{ac}. The $R_{ON} \cdot A$ versus L_{ac} curve follows a parabolic relationship, as an increase in L_{ac} results in a proportional increase of both the R_{ON} and the A. The V_B versus L_{ac} curve follows a linear relationship and reaches 22.5 kV for $L_{ac} = 100$ μm. The ability of scaling the V_B to more than 20 kV suggests this device structure a promising candidate for making medium voltage power switches.

C. Performance Benchmarking of Multichannel SHJ Diodes

By stacking multiple GaN/AlGaN/GaN structures vertically, $R_{ON} \cdot A$ can be reduced while keeping the same V_B. Fig. 5 shows the tradeoff relationship between $R_{ON} \cdot A$ and V_B for SHJ Schottky diodes with different L_{ac} and number of channels. Theoretical 1-D unipolar limits for Si, SiC, and GaN materials and the GaN SHJ limit for single channel are

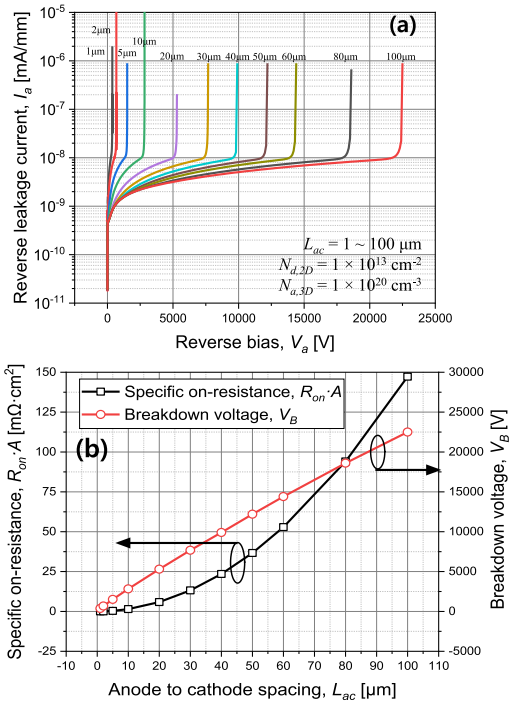

Fig. 4. (a) Reverse I–V characteristics of charge-balanced GaN/AlGaN/GaN single-channel Schottky diodes with different L_{ac}. (b) $R_{ON} \cdot A$ and V_B characteristics as a function of L_{ac}.

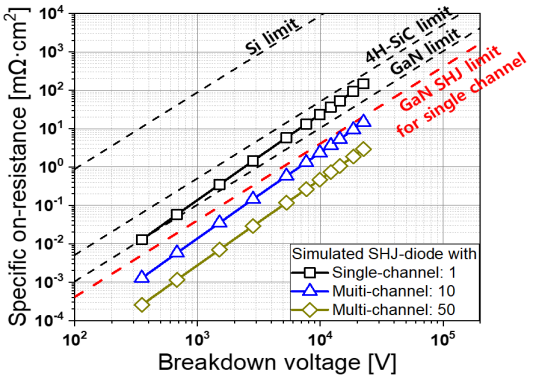

Fig. 5. Tradeoff relationship between $R_{ON} \cdot A$ and V_B of charge-balanced single- and multichannel SHJ Schottky diodes designed for 0.35–22.5 kV applications. Theoretical limits for Si, 4H-SiC, and GaN materials and the GaN SHJ limit for single channel are included.

shown on the same plot as references. With single-channel SHJ, the simulated performance of the diode is reaching the 1-D unipolar limit of GaN. By stacking multiple SHJ channels, the simulated device performance can far exceed that limit. For example, with ten channels, a 10-kV device can have a $R_{ON} \cdot A$ as low as 2.5 mΩ·cm^2, which is a factor of 20× better than the theoretical limit of conventional SiC MOSFETs and a factor of 50× better than the SiC MOSFET experimental performance results [15].

We also derived the analytical tradeoff relationship between $R_{ON} \cdot A$ and V_B for the GaN SHJ structure. The derivation starts with a charge-balanced single-channel SHJ structure (p-GaN/delta-doped n-GaN/p-AlGaN/p-GaN). At OFF-state, the SHJ structure is fully depleted across the vertical pn heterojunction. In the charge-balanced structure (i.e., $N_{d,2\text{-D}} = 2N_{a,3\text{-D}} \cdot t_{GaN}$), the maximum E-field in the y-direction in GaN is given by

$$|E_y|_{\max,GaN} = \frac{q \cdot \frac{1}{2} \cdot N_{d,2\text{-D}}}{\varepsilon_{GaN}} = \frac{q \cdot N_{a,3\text{-D}} \cdot t_{GaN}}{\varepsilon_{GaN}} \quad (1.1)$$

and in the y-direction AlGaN is given by

$$|E_y|_{\max.\mathrm{AlGaN}} = \frac{q \cdot N_{a,3\text{-D}} \cdot t_{\mathrm{GaN}}}{\varepsilon_{\mathrm{GaN}}} - \frac{(\sigma_{\mathrm{AlGaN}} - \sigma_{\mathrm{GaN}})}{\varepsilon_{\mathrm{AlGaN}}} \quad (1.2)$$

where q, $\varepsilon_{\mathrm{GaN}}$, $\varepsilon_{\mathrm{AlGaN}}$, σ_{GaN}, and σ_{AlGaN} are unit charge, permittivity, and polarization charge of GaN and AlGaN, respectively. In (1.2), the polarization E-field term "$(\sigma_{\mathrm{AlGaN}} - \sigma_{\mathrm{GaN}})/\varepsilon_{\mathrm{AlGaN}}$" is determined by the Al composition. It has an opposite direction from the E-field induced by the pn heterojunction space charges. Although the maximum E-field "$|E|_{\max} = (E_{x.\max}^2 + E_{y.\max}^2)^{1/2}$" in AlGaN could be higher than $|E|_{\max}$ in GaN, AlGaN has a much higher critical field $E_{c.\mathrm{AlGaN}}$ than $E_{c.\mathrm{GaN}}$. Our calculation suggests that breakdown will always occur in the GaN. When $|E|_{\max}$ in GaN reaches the $E_{\mathrm{C.GaN}}$, the y component of the maximum E-field can be expressed as a faction of the $E_{\mathrm{C.GaN}}$, given by

$$|E_y|_{\max} = \frac{q \cdot \frac{1}{2} \cdot N_{d,2\text{-D}}}{\varepsilon_{\mathrm{GaN}}} = \frac{q \cdot N_{a,3\text{-D}} \cdot t_{GaN}}{\varepsilon_{\mathrm{GaN}}} = \alpha \cdot E_{C.\mathrm{GaN}} \quad (2)$$

where α is a factor with its value between 0 and 1. With the superjunction design, the lateral E-field (E_x) at OFF-state is approximately a constant value between the cathode and the anode as confirmed later by simulation results shown in Fig. 10. When the device reaches its breakdown voltage, the E_x can be written as

$$V_{\mathrm{B}} = |E_x|_{\max} \cdot L_{AC} = \beta \cdot E_C \cdot L_{AC} \quad (3.1)$$

where β is the factor with its value between 0 and 1. Factors α and β are related to each other through

$$\alpha^2 + \beta^2 = 1. \quad (3.2)$$

When the device is in thermal equilibrium, from the charge neutrality equation, we can derive that the density of the 2DEG is given by the difference of positive charge density (i.e., delta-doping density) and the negative charge density (i.e., acceptor density in the depletion region integrated over the depletion width)

$$n_s = N_{d,2\text{-D}} - 2 \cdot N_{a,3\text{-D}} \cdot w_D \quad (4)$$

where w_D is the depletion width of vertical p-n heterojunction in thermal equilibrium. Since n-type doping volume density is much higher than the p-type doping density, the p-n junction can be treated as one-sided. The w_D can be written as

$$w_D = \sqrt{\frac{2 \cdot V_{\mathrm{bi}} \cdot \varepsilon_{\mathrm{GaN}}}{q \cdot N_{a,3\text{-D}}}}. \quad (5)$$

The $R_{\mathrm{ON}} \cdot A$ of the single-channel SHJ structure can be expressed as

$$R_{\mathrm{ON}} \cdot A = R_s \cdot \frac{L_{\mathrm{ac}}}{W_{\mathrm{ch}}}(L_{\mathrm{ac}} \cdot W_{\mathrm{ch}}) = \frac{1}{q \cdot n_s \cdot \mu_s} L_{\mathrm{ac}}^2 = \frac{1}{q(N_{d,2\text{-D}} - 2 \cdot N_{a,3\text{-D}} \cdot w_D)\mu_s} L_{\mathrm{ac}}^2 \quad (6)$$

where R_s, μ_s, and W_{ch} are sheet resistance of 2DEG, sheet mobility of 2DEG, and 2DEG channel width (i.e., dimension in z-direction). Substituting (2), (3.1), (3.2), and (5) into (6) and considering the stacking of multiple 2DEG channels, the $R_{\mathrm{ON}} \cdot A$ for the multichannel GaN SHJ structure can be derived by

$$R_{\mathrm{ON}} \cdot A = \frac{1}{2\alpha(1-a^2)} \frac{1}{n_{\mathrm{ch}}} \frac{V_{\mathrm{B}}^2}{\left(1 - \sqrt{\frac{2V_{\mathrm{bi}}}{\alpha \cdot E_{c.\mathrm{GaN}} \cdot t_{\mathrm{GaN}}}}\right) \mu_s \cdot \varepsilon_{GaN} \cdot E_{C.\mathrm{GaN}}^3} \quad (7)$$

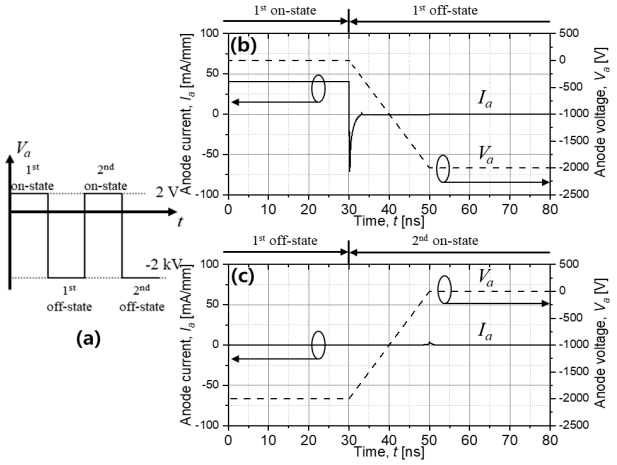

Fig. 6. (a) Schematic of the anode voltage waveform setup for the simulation. (b) Simulated turn-off (between first ON-state and first OFF-state). (c) Turn-on (between first OFF-state and second ON-state) transient switching waveforms of charge-balanced single-channel SHJ Schottky diode.

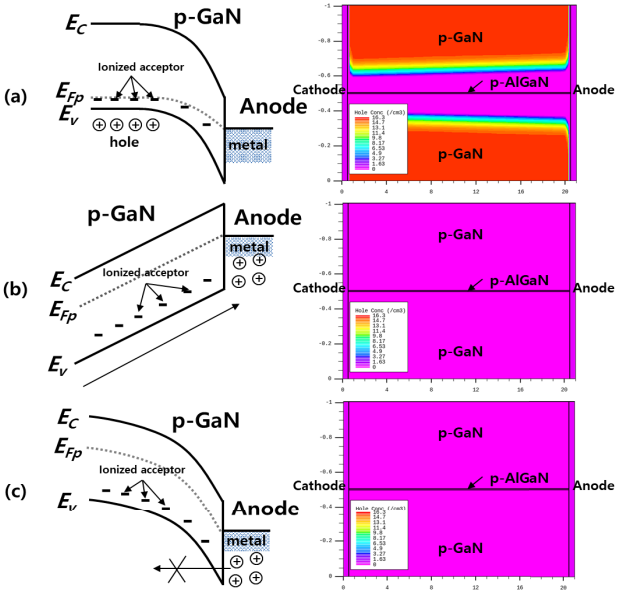

Fig. 7. Schematic of band energy diagram at anode/p-GaN junction and simulated hole concentration contours in (a) first ON-state: $V_a = 2$ V, (b) first OFF-state: $V_a = -2$ kV, and (c) second ON-state: $V_a = 2$ V during the transient switching.

where n_{ch} is the number of 2DEG channels. From (7), we can conclude that a large p-GaN thickness t_{GaN} is preferred to minimize the ON-resistance, without sacrificing anything else. The ideal specific ON-resistance of SHJ structure as a function of V_{B} are derived, whereas $R_{\mathrm{ON}} \cdot A$ has a minimum value by optimizing the value of the α factor

$$R_{\mathrm{ON}} \cdot A = \frac{3\sqrt{3}}{4} \frac{1}{n_{\mathrm{ch}}} \frac{V_{\mathrm{B}}^2}{\mu_s \cdot \varepsilon_{\mathrm{GaN}} \cdot E_{C.\mathrm{GaN}}^3}, \quad \text{when } a = \sqrt{\frac{1}{3}}. \quad (8)$$

With the α factor at its optimum value, we can find from (2) that the optimum n-typing doping density $N_{d.2\text{-D}} = 1.9 \times 10^{13}$ cm^{-2}. High $N_{d.2\text{-D}}$ would require a thick AlGaN with high Al composition to transfer the electrons from the doped region to the 2DEG channel, at the risk of exceeding the critical thickness of the AlGaN. In this work, we used a conservative $N_{d.2\text{-D}}$ value of 1×10^{13} cm^{-2}.

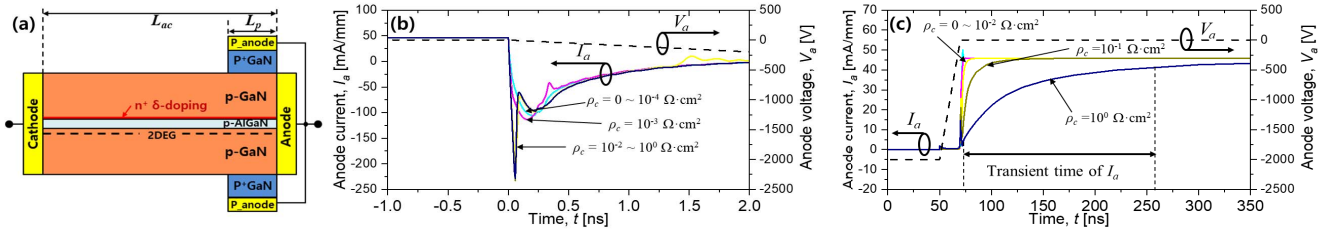

Fig. 8. (a) Schematics of single-channel SHJ Schottky diode with p-ohmic anode electrodes. (b) Simulated turn-off (between first ON-state and first OFF-state). (c) Turn-on (between first OFF-state and second ON-state) transient switching waveforms for SHJ Schottky diodes having p-ohmic anode electrode with different p-type ohmic contact resistivity values.

D. Transient Switching Characteristics of SHJ-Diode

We performed a transient switching simulation to evaluate the dynamic performance of the proposed SHJ diode. The SHJ diode used for transient simulation was a single-channel GaN/AlGaN/GaN SHJ, where L_{ac}, t_{AlGaN}, $N_{d,\text{2-D}}$, and $N_{a,\text{3-D}}$ were 20 μm, 5 nm, 1×10^{13} cm^{-2}, and 1×10^{17} cm^{-3}, respectively. This structure yielded a simulated avalanche breakdown voltage of 5.3 kV. Fig. 6(a) shows a schematic of the anode voltage waveform used for the simulation. The switching frequency, duty ratio, and switching transient time were 1 MHz, 50%, and 20 ns (~100 V/ns), respectively. The forward and reverse biases for the transient switching were 2 V and –2 kV. Fig. 6(b) and (c) shows the simulated turn-off (between first ON-state and first OFF-state) and turn-on (between first OFF-state and second ON-state) transient switching waveforms of the SHJ diode. The forward current of the SHJ diode was 43 mA/mm in the first ON-state, consistent with the static forward current. During the on-to-off transition, a negative current spike appeared corresponding to the reverse recovery process. During the off-to-on transition, the diode could not be turned on, with a forward current value as low as 5 μA/mm.

The inability of switching the diode from OFF-state to ON-state is due to the difficulty in supplying holes to the SHJ. To explain the mechanism, we illustrated band diagrams at the anode/p-GaN junction and simulated hole concentration contours of the SHJ diode in Fig. 7. During the first ON-state [Fig. 7(a),$V_a = 2$ V], there were large amounts of electrons and holes in the structure. The electrons provided a forward conduction path. Once the SHJ diode was reverse biased [Fig. 7(b), $V_a = -2$ kV], all holes in the p-type region were depleted out through the anode by the E-field, leaving behind negatively charged acceptors. Similarly, all electrons in the system were depleted out through the cathode, leaving behind positively charged donors. The charge balance between ionized acceptors and donors is the key to superjunction operation. When the diode was switched from the first OFF-state to the second ON-state [Fig. 7(c), $V_a = 2$ V], the supply of holes from the anode back into the p-type region was blocked by the Schottky barrier between the anode and the semiconductor. The p-type region remained negatively charged, preventing the supply of electrons from the cathode back into the semiconductor. From this analysis, the SHJ concept is not able to switch without a proper p-type contact made to the structure to supply holes.

IV. SHJ Diode With p-Type Ohmic Anode Electrodes

The serious switching problem can be solved by adding a p-type ohmic anode electrode. Through the p-type ohmic anode electrode, holes can be injected back into the semiconductor during the off-to-on switching transient. Injected holes neutralize the acceptors, thereby allowing electrons to be supplied to the semiconductor through the cathode, forming forward current conduction channel. It is important that p-type ohmic contacts are formed to all p-GaN layers, as shown in Fig. 1. Only adding p-type ohmic contact to the top p-GaN layer will fail to supply holes to the lower p-GaN layers separated by the 2DEG, even under a large forward bias. This is because the short minority carrier lifetime makes it extremely hard for the injected holes to diffuse across the n-type region. Using a simplified structure shown in Fig. 8(a), we evaluated the impact of a p-type ohmic anode on device characteristics through 2-D simulation. L_{ac} and length of the p-anode region were 20 and 2 μm, respectively. The anode and the p-anode are electrically connected. Other structural parameters are the same as those used in the previous transient simulation. Simulated switching waveforms shown in Fig. 8(b) and (c) suggest that problem in off-to-on switching was fixed by adding the p-type ohmic contacts. Contact resistivity of the p-type ohmic contacts affects the turn-on time. For a p-type ohmic contact resistivity of $1 \times 10^{-7} \sim 1\ \Omega \cdot \text{cm}^2$, turn-on time of the anode current rising from 10% to 90% was 0.1–210 ns, sufficient for most of the power electronics applications. In practice, p-type ohmic resistivity ranging from $1 \times 10^{-6}\Omega \cdot \text{cm}^2$ to $1 \times 10^{-4}\Omega \cdot \text{cm}^2$ can be routinely achieved on as-grown p-GaN surface [16]. However, forming p-type ohmic contacts on the etched surface has been very challenging, due to the formation of donor-like nitrogen vacancies caused by plasma damage [17], [18]. Regrowth of p$^+$-GaN on the etched p-GaN sidewall is needed to form p-type ohmic contacts [19] to all p-GaN layers in the multichannel SHJ structure. As the p-anode electrode was added, the "effective L_{ac}" ($L_{\text{ac}} - L_p$) of the SHJ diode decreased by L_p. The forward current improved with the addition of the p-type ohmic anode as shown in Fig. 9(a). The improvement of forward current was due to

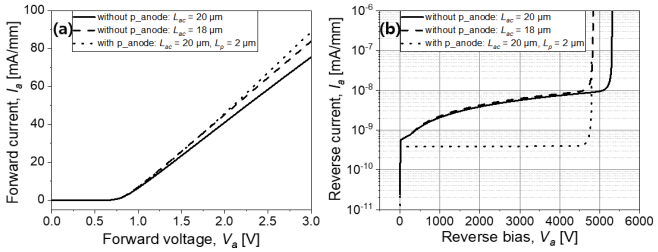

Fig. 9. Comparison of (a) forward and (b) reverse I–V characteristics of three different diode structures: solid line [SHJ-diode without p-anode electrodes ($L_{\text{ac}} = 20\ \mu$m)], dashed line [SHJ-diode without p-anode electrodes ($L_{\text{ac}} = 18\ \mu$m)], and dotted line [SHJ diode with p-anode electrodes ($L_{\text{ac}} = 20\ \mu$m, $L_p = 2\ \mu$m)].

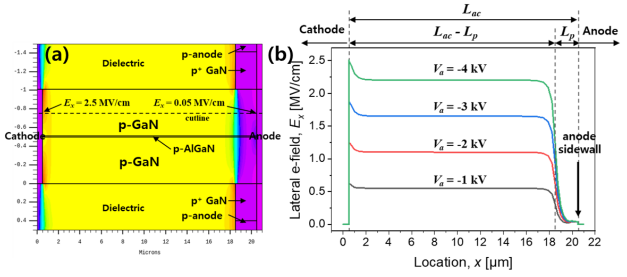

Fig. 10. (a) Simulated 2-D lateral E-field contour of SHJ-diode with p-ohmic anode electrode [at $V_a = -4$ kV]. (b) Cutline 1-D lateral e-filed distribution with a different reverse bias.

the combined effects of a shorter effective L_{ac} and conductivity modulation provided by the forward-biased p-n junction. With the addition of the p-type ohmic anode electrodes, the V_B decreased slightly, consistent with the reduction of the effective L_{ac}, as shown in Fig. 9(b). Meanwhile, the leakage current was substantially reduced as compared with the structure without the p-type ohmic contacts. The low and flat reverse leakage characteristics can be explained by the E-field distribution. Fig. 10(a) shows the lateral E-field contour of SHJ diode with p-anode structure at $V_a = -4$ kV. The p-anode electrodes clamped the lateral E-field at the Schottky junction at a very low value 0.05 MV/cm, as compared with the high value of 2.5 MV/cm in the device without the p-anodes. Drastic reduction of E-field at the Schottky junction resulted in a large reduction of thermionic field emission current, which is the dominating reverse leakage current mechanism [20]. Fig. 10(b) shows a 1-D lateral cutline of simulated E-field distribution with different reverse biases. The E-field was about constant along the effective L_{ac} direction and decreased rapidly under the p-anodes. The average E-field of the device increases linearly with the increase in the reverse voltage.

V. Conclusion

We investigated several key design aspects of GaN multichannel SHJ. With n-type doping, high-density 2DEG can be formed in each channel of the GaN/AlGaN/GaN multichannel structure without the need for using the AlGaN layer with a high Al composition or large thickness, making it easier to scale to a larger number of channels before reaching the critical thickness. p-type doping is needed to balance the n-type doping and achieve the maximum V_B. p-type ohmic contacts to each p-type GaN layer is needed to ensure proper switching behaviors. The resulting GaN/AlGaN/GaN multichannel SHJ has the potential to well exceed the 1-D unipolar performance limit of SiC and GaN. While the work described in this article was based on a diode structure, the conclusions are applicable to transistor structures as well.

References

[1] H. Amano *et al.* "The 2018 GaN power electronics roadmap," *J. Phys. D, Appl. Phys.*, vol. 51, Mar. 2018, Art. no. 163001, doi: 10.1088/1361-6463/aaaf9d.

[2] F. Udrea, G. Deboy, and T. Fujihira, "Superjunction power devices, history, development, and future prospects," *IEEE Trans. Electron Devices*, vol. 64, no. 3, pp. 720–734, Mar. 2017, doi: 10.1109/TED.2017.2658344.

[3] Z. Li and T. P. Chow, "Design and simulation of 5–20-kV GaN enhancement-mode vertical superjunction HEMT," *IEEE Trans. Electron Devices*, vol. 60, no. 10, pp. 3230–3237, Oct. 2013, doi: 10.1109/TED.2013.2266544.

[4] M. Xiao, R. Zhang, D. Dong, H. Wang, and Y. Zhang, "Design and simulation of GaN superjunction transistors with 2-DEG channels and fin channels," *IEEE J. Emerg. Sel. Topics Power Electron.*, vol. 7, no. 3, pp. 1475–1484, Sep. 2019, doi: 10.1109/JESTPE.2019.2912978.

[5] Y. Oonishi, A. Ooi, and T. Shimatou, "Superjunction MOSFET," *Fuji Electron. Rev.*, vol. 56, no. 2, pp. 65–68, 2000.

[6] S. Yamauchi, T. Shibata, S. Nogami, T. Yamaoka, Y. Hattori, and H. Yamaguchi, "200V super junction MOSFET fabricated by high aspect ratio trench filling," in *Proc. IEEE Int. Symp. Power Semicond. Devices IC's*, Jun. 2006, pp. 1–4, doi: 10.1109/ISPSD.2006.1666072.

[7] J. H. Ryou *et al.*, "Surface treatment on the growth surface of semi-insulating GaN bulk substrate for III-nitride heterostructure field-effect transistors," *Phys. Status Solidi*, vol. 5, no. 6, pp. 1849–1851, 2008, doi: 10.1002/pssc.200778698.

[8] Y.-Y. Wong *et al.*, "Effect of nitridation on the regrowth interface of AlGaN/GaN structures grown by molecular beam epitaxy on GaN templates," *J. Electron. Mater.*, vol. 41, no. 8, pp. 2139–2144, 2012, doi: 10.1007/s11664-012-2150-2.

[9] H. Ishida *et al.*, "Unlimited high breakdown voltage by natural super junction of polarized semiconductor," *IEEE Electron Device Lett.*, vol. 29, no. 10, pp. 1087–1089, Oct. 2008, doi: 10.1109/LED.2008.2002753.

[10] J. P. Ibbetson, P. T. Fini, K. D. Ness, S. P. DenBaars, J. S. Speck, and U. K. Mishra, "Polarization effects, surface states, and the source of electrons in AlGaN/GaN heterostructure field effect transistors," *Appl. Phys. Lett.*, vol. 77, no. 2, pp. 250–252, 2000, doi: 10.1063/1.126940.

[11] A. Xie, E. Beam, and Y. Cao, "Growth and characterization of GaN based multi-channel FETs," in *Proc. 235th ECS Meeting*, Dallas, TX, USA, May 2019, p. 1277.

[12] B. Mazumder, M. H. Wong, C. A. Hurni, J. Y. Zhang, U. K. Mishra, and J. S. Speck, "Asymmetric interfacial abruptness in N-polar and Ga-polar GaN/AlN/GaN heterostructures," *Appl. Phys. Lett.*, vol. 101, no. 9, Aug. 2012, doi: 10.1063/1.4748116.

[13] S. R. Lee *et al.*, "In situ measurements of the critical thickness for strain relaxation in AlGaN/GaN heterostructures," *Appl. Phys. Lett.*, vol. 85, no. 25, pp. 6164–6166, 2004, doi: 10.1063/1.1840111.

[14] H. V. Stanchu *et al.*, "Local strain and crystalline defects in GaN/AlGaN/GaN(0001) heterostructures induced by compositionally graded AlGaN buried layers," *Cryst. Growth Des.*, vol. 19, no. 1, pp. 200–210, 2019, doi: 10.1021/acs.cgd.8b01267.

[15] S.-H. Ryu *et al.*, "10-kV, 123-m$\Omega\cdot$cm^2 4H-SiC power DMOSFETs," *IEEE Electron Device Lett.*, vol. 25, no. 8, pp. 556–558, Aug. 2004, doi: 10.1109/LED.2004.832122.

[16] J. Chen and W. D. Brewer, "Ohmic contacts on p-GaN," *Adv. Electron. Mater.*, vol. 1, no. 8, 2015, Art. no. 1500113, doi: 10.1002/aelm.201500113.

[17] S. Hautakangas *et al.*, "Vacancy defects as compensating centers in Mg-Doped GaN," *Phys. Rev. Lett.*, vol. 90, no. 13, 2003, Art. no. 137402, doi: 10.1103/PhysRevLett.90.137402.

[18] X. A. Cao *et al.*, "Electrical effects of plasma damage in p-GaN," *Appl. Phys. Lett.*, vol. 75, no. 17, pp. 2569–2571, Oct. 1999, doi: 10.1063/1.125080.

[19] D. Shibata *et al.*, "1.7 kV/1.0 m$\Omega\cdot$cm^2 normally-off vertical GaN transistor on GaN substrate with regrown p-GaN/AlGaN/GaN semipolar gate structure," in *IEDM Tech. Dig.*, Dec. 2016, pp. 10.1.1–10.1.4, doi: 10.1109/IEDM.2016.7838385.

[20] D. Shibata *et al.*, "GaN-based multi-junction diode with low reverse leakage current using p-type barrier controlling layer," in *IEDM Tech. Dig.*, Dec. 2011, pp. 26.2.1–26.2.4, doi: 10.1109/IEDM.2011.6131616.

[21] M. Farahmand *et al.*, "Monte Carlo simulation of electron transport in the III-nitride wurtzite phase materials system: Binaries and ternaries," *IEEE Trans. Electron Devices*, vol. 48, no. 3, pp. 535–542, Mar. 2001, doi: 10.1109/16.906448.

[22] S. Selberherr, *Analysis and Simulation of Semiconductor Devices*. New York, NY, USA: Springer-Verlag, 1984.

[23] Z. Z. Bandić, P. M. Bridger, E. C. Piquette, and T. C. McGill, "Electron diffusion length and lifetime in p-type GaN," *Appl. Phys. Lett.*, vol. 73, no. 22, pp. 3276–3278, 1998, doi: 10.1063/1.122743.

[24] Z. Z. Bandić, P. M. Bridger, E. C. Piquette, and T. C. McGill, "Minority carrier diffusion length and lifetime in GaN," *Appl. Phys. Lett.*, vol. 72, no. 24, pp. 3166–3168, 1998, doi: 10.1063/1.121581.

[25] *TCAD Examples: Blue Single Quantum Well GaN LED*. Accessed: Aug. 28, 2019. [Online]. Available: https://www.silvaco.com/examples/tcad/section22/example3